Comput Mech (2011) 47:395–408
DOI 10.1007/s00466-010-0550-9

ORIGINAL PAPER

The vibrations of pre-twisted rotating Timoshenko beams by the Rayleigh–Ritz method

T.-L. Zhu

Received: 2 July 2010 / Accepted: 25 October 2010 / Published online: 11 November 2010

Abstract A modeling method for flapwise and chordwise bending vibration analysis of rotating pre-twisted Timoshenko beams is introduced. In the present modeling method, the shear and the rotary inertia effects on the modal characteristics are correctly included based on the Timoshenko beam theory. The kinetic and potential energy expressions of this model are derived from the Rayleigh–Ritz method, using a set of hybrid deformation variables. The equations of motion of the rotating beam are derived from the kinetic and potential energy expressions introduced in the present study. The equations thus derived are transmitted into dimensionless forms in which main dimensionless parameters are identified. The effects of dimensionless parameters such as the hub radius ratio, slenderness ration, etc. on the natural frequencies and modal characteristics of rotating pre-twisted beams are successfully examined through numerical studies. Finally the resonance frequency of the rotating beam is evaluated.

Keywords Modal characteristics · Pre-twisted rotating Timoshenko beams · Hybrid deformation variables · Dimensionless parameters · Rayleigh–Ritz method

1 Introduction

Pre-twisted rotating beams have been widely used in engineering structures such as turbines, wind blades, aircraft rotary wings, etc. Proper evaluation of their modal characteristics is critical to the design and analysis of these rotating structures. The modal characteristics of rotating beams often vary significantly from those of non-rotating beams due to the influence of centrifugal inertia force. Due to this significant variation of modal characteristics resulted from rotation, the modal characteristics of rotating beams have been widely investigated.

The initial investigations were mainly focused on non-twisted rotating beams. An early analytical method to calculate the natural frequencies of a rotating beam was presented by Southwell and Gough [1]. Based on the Rayleigh energy theorem, an equation, known as the Southwell equation, that relates the natural frequency to the rotating frequency of a beam was developed. This study was further extended by Liebers [2], Theodorsen [3] and Schilhansl [4], to obtain more accurate natural frequencies of rotating beams. However, due to the large amount of calculation and lack of computational devices, the mode shapes were not available in these investigations. Later, using digital computers, investigations in mode shapes and more accurate natural frequencies were published for rotating beams. These investigations include the assumed mode method [5], the vibrations of non-uniform beams [6,7], the effect of tip mass on natural frequencies [8,9], the effect of offset root [10], the effect of shear deformation [11], the effect of shear deformation and elastic foundation [12], the gyroscopic damping effect [13], and the taper effect [14].

The effect of a pre-twist angle on the modal characteristics of cantilever beams was also widely investigated. Dawson [15] and Dawson and Carnegie [16] used the Rayleigh–Ritz method to investigate the effects of a uniform twist on the natural frequencies of a uniform cantilever blade. Carnigie and Thomas [17] extended the Rayleigh–Ritz method developed in [15] and [16] to the analysis of tapered blades with uniform pretwist. Dokumaci et al. [18] used a matrix displacement analysis to study the vibrations of pretwisted blades. Rao [19] and Gupta and Rao [20] used the Ritz–Galerkin method and finite element method to study the effects of pretwist

T.-L. Zhu (✉)
Department of Mechanical Engineering, Widener University, One University Place, Chester, PA 19013, USA
e-mail: tzhu@mail.widener.edu

on the natural frequencies of cantilever blades. Celep and Turhan [21] used a Galerkin approach to investigate the effect of shear deformation and non-uniform pretwist on the natural frequencies of beams. Lin [22] employed a generalized transfer matrix method to investigate the modal characteristics of beams with arbitrary pretwist. However the effects created by the rotational motion were not considered in the above studies. Ramamurti and Kielb [23] employed a plate theory to calculate the natural frequency of rotating pre-twisted beams. Subrahmanyam and Kaza [24] investigated the modal characteristics of rotating pretwisted beams, using the Ritz method and finite difference method. Subrahmanyam et al. [25] used the Reissner method to study the modal characteristics of rotating pretwisted beams. Lin [26] investigated the frequencies of a rotating pretwisted beams with elastically restrained root. Lin et al. [27] investigated the natural frequencies of rotating non-uniform twist beams with an elastically restrained root and a tip mass.

Most of the above modeling approaches used the popular classical linear modeling method [28,29]. Recently, a new dynamic modeling method which employs a hybrid set of deformation variables was introduced in Kane et al. [30], Yoo et al. [31,32], for the vibration analysis of Euler–Bernoulli beams. Full sets of linearized equations of motion were derived using the hybrid set of deformation variables. The linear equations, different from those from the classical linear modeling method, were shown to provide proper stiffness variation due to rotational motion. Yoo et al. [33] extended the approach to the analysis of the flapwise bending vibration of a rotating composite beams, including the effects of the shear and rotary inertia, but several terms were missed in the kinetic energy in their development.

In the present study, the equations of motion of rotating pre-twisted Timoshenko beams are derived using the hybrid deformation variables proposed in Yoo et al. [31,32]. The present study will include the effects of shear and rotary inertia on the modal characteristics of the rotating pre-twisted beams. The combined effect of angular speed, hub radius, slenderness ratio, effective shear to axial modulus ratio on the modal characteristics of a rotating Timoshenko beam is successfully investigated in this study.

2 Equations of motion

2.1 Approximation of deformation variables

The following assumptions are made in the present work so as to simplify the formulations and to focus on the critical effects due to rotation. The material of the Timoshenko beam is homogeneous and isotropic. The pre-twist rate of the beam along its longitudinal axis is uniform. The gyroscopic coupling between the stretching and bending motions

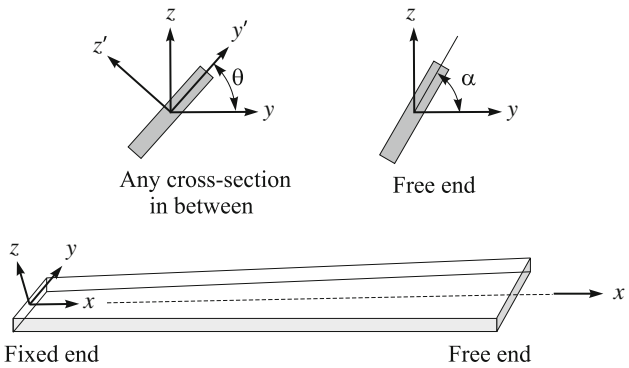

Fig. 1 Configuration of a pre-twisted beam

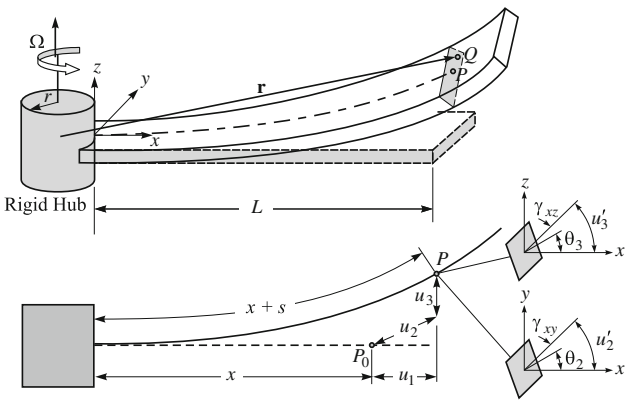

Fig. 2 Deformation of the beam and the neutral axis

is negligible. The neutral and centroidal axes in the cross-section of the beam coincide so that neither eccentricity nor torsion needs to be considered.

Figure 1 shows the configuration of a uniformly pre-twisted beam. α is the pre-twist angle at the free end of the beam (where a rotating coordinate system XYZ, with its unit vectors $\mathbf{i}'$, $\mathbf{j}'$ and $\mathbf{k}'$, is attached) with respect to the fixed end (where another rotating coordinate system xyz, with its orthogonal unit vectors $\mathbf{i}$, $\mathbf{j}$ and $\mathbf{k}$, is attached).

Figure 2 shows the deformation of the beam and the deformation of the neutral axis of the beam. A generic point P_0 which lies on the undeformed neutral axis moves to P when the beam is deformed. Three Cartesian variables u_1, u_2 and u_3 are shown to describe the deformation of Point P. θ_2 and θ_3 are the rotational angles of the cross-section in the $x-y$ and $x-z$ planes, respectively. The stretch of the arc length of the neutral axis, s is also shown in Fig. 2. The arc length stretch, s, a non-Cartesian variable will be used, instead of u_1, to compute the strain and kinetic energies. The strains and rotational angles at each cross-section of the beam are also shown in the figure.

There is a geometric relation between the arc length stretch s and the Cartesian variables. This relation is later used

to derive the generalized inertia forces in the equations of motion. In Ref. [34], the relation is given as

$$s = u_1 + \frac{1}{2}\int_0^x \left[\left(u_2'\right)^2 + \left(u_3'\right)^2\right] d\sigma \tag{1}$$

or

$$u_1 = s - \frac{1}{2}\int_0^x \left[\left(u_2'\right)^2 + \left(u_3'\right)^2\right] d\sigma \tag{2}$$

where a symbol with a prime ($'$) represents the partial derivative with respect to the integral domain variable.

In the present work, s, u_2, θ_2, u_3 and θ_3 are approximated by spatial functions and the corresponding coordinates. By employing the Rayleigh Ritz method, the deformation variables are approximated as follows

$$s(x,t) = \sum_{j=1}^{\mu_1} \phi_{1j}(x) q_{1j}(t) \tag{3}$$

$$u_2(x,t) = \sum_{j=1}^{\mu_2} \phi_{2j}(x) q_{2j}(t) \tag{4}$$

$$\theta_2(x,t) = \sum_{j=1}^{\mu_3} \phi_{3j}(x) q_{3j}(t) \tag{5}$$

$$u_3(x,t) = \sum_{j=1}^{\mu_4} \phi_{4j}(x) q_{4j}(t) \tag{6}$$

$$\theta_3(x,t) = \sum_{j=1}^{\mu_5} \phi_{5j}(x) q_{5j}(t) \tag{7}$$

In the above equations, $\phi_{1j}, \phi_{2j}, \phi_{3j}, \phi_{4j}$ and ϕ_{5j} are the assumed modal functions (test functions) for s, u_2, θ_2, u_3, and θ_3, respectively. Any compact set of functions which satisfy the essential boundary conditions of the Timoshenko beam can be used as the test functions. The q_{ij}s are the generalized coordinates and $\mu_1, \mu_2, \mu_3, \mu_4$, and μ_5 are the number of assumed modes used for s, u_2, θ_2, u_3, and θ_3, respectively. The total number of modes, μ, equals the summation of these individual number of modes, i.e.,

$$\mu = \mu_1 + \mu_2 + \mu_3 + \mu_4 + \mu_5 \tag{8}$$

2.2 The strain energy of the system

The elastic strain energy of a Timoshenko beam, employing the hybrid set of deformation variables, is given by [35]

$$U = \frac{1}{2}\int_0^L \left[EA\left(\frac{\partial s}{\partial x}\right)^2 + EI_3\left(\frac{\partial \theta_2}{\partial x}\right)^2 + EI_2\left(\frac{\partial \theta_3}{\partial x}\right)^2 + 2EI_{23}\frac{\partial \theta_2}{\partial x}\frac{\partial \theta_3}{\partial x} + k_2AG\left(\theta_2 - \frac{\partial u_2}{\partial x}\right)^2 + k_3AG\left(\theta_3 - \frac{\partial u_3}{\partial x}\right)^2\right] dx \tag{9}$$

where E is the Young's modulus, G is the shear modulus, k_2 and k_3 are the shear correction factors, A is the cross-sectional area of the beam, I_2, I_3 and I_{23} are the second area moments of inertia and the second area products of inertia of the cross-section, respectively, and L is the length of the beam. By using I_2^* and I_3^*, the principal second area moments of the cross-section, I_2, I_3 and I_{23} can be expressed as follows

$$I_2(x) = \frac{I_2^* + I_3^*}{2} + \frac{I_2^* - I_3^*}{2}\cos(2\theta) \tag{10}$$

$$I_3(x) = \frac{I_2^* + I_3^*}{2} - \frac{I_2^* - I_3^*}{2}\cos(2\theta) \tag{11}$$

$$I_{23}(x) = \frac{I_2^* - I_3^*}{2}\sin(2\theta) \tag{12}$$

where

$$\theta = \alpha\frac{x}{L} \tag{13}$$

is the pre-twist angle of a cross-section with respect to the fixed end. Thus $\theta = 0$ at the fixed end and $\theta = \alpha$ at the free end.

Substituting Eqs. (3)–(7) into Eq. (9), one obtains

$$U = \frac{1}{2}\int_0^L \left[EA\left(\sum_{j=1}^{\mu_1}\phi_{1j}'q_{1j}\right)^2 + EI_3\left(\sum_{j=1}^{\mu_3}\phi_{3j}'q_{3j}\right)^2 + EI_2\left(\sum_{j=1}^{\mu_5}\phi_{5j}'q_{5j}\right)^2 + 2EI_{23}\left(\sum_{j=1}^{\mu_3}\phi_{3j}'q_{3j}\right)\left(\sum_{j=1}^{\mu_5}\phi_{5j}'q_{5j}\right) + k_2AG\left(\sum_{j=1}^{\mu_3}\phi_{3j}q_{3j} - \sum_{j=1}^{\mu_2}\phi_{2j}'q_{2j}\right)^2 + k_3AG\left(\sum_{j=1}^{\mu_5}\phi_{5j}q_{5j} - \sum_{j=1}^{\mu_4}\phi_{4j}'q_{4j}\right)^2\right] dx \tag{14}$$

The partial derivatives of U with respect to q_{1i}, q_{2i}, q_{3i}, q_{4i} and q_{5i} can then be obtained as

$$\frac{\partial U}{\partial q_{1i}} = \int_0^L EA \sum_{j=1}^{\mu_1} \phi'_{1i}\phi'_{1j}q_{1j}dx \tag{15}$$

$$\frac{\partial U}{\partial q_{2i}} = \int_0^L k_2AG\left(\sum_{j=1}^{\mu_2}\phi'_{2i}\phi'_{2j}q_{2j} - \sum_{j=1}^{\mu_3}\phi'_{2i}\phi_{3j}q_{3j}\right)dx \tag{16}$$

$$\begin{aligned}\frac{\partial U}{\partial q_{3i}} = \int_0^L \Bigg[& EI_3\left(\sum_{j=1}^{\mu_3}\phi'_{3i}\phi'_{3j}q_{3j}\right) \\ & + EI_{23}\left(\sum_{j=1}^{\mu_5}\phi'_{3i}\phi'_{5j}q_{5j}\right) \\ & + k_2AG\left(\sum_{j=1}^{\mu_3}\phi_{3i}\phi_{3j}q_{3j} - \sum_{j=1}^{\mu_2}\phi_{3i}\phi'_{2j}q_{2j}\right)\Bigg]dx\end{aligned} \tag{17}$$

$$\frac{\partial U}{\partial q_{4i}} = \int_0^L k_3AG\left(\sum_{j=1}^{\mu_4}\phi'_{4i}\phi'_{4j}q_{4j} - \sum_{j=1}^{\mu_5}\phi'_{4i}\phi_{5j}q_{5j}\right)dx \tag{18}$$

$$\begin{aligned}\frac{\partial U}{\partial q_{5i}} = \int_0^L \Bigg[& EI_2\left(\sum_{j=1}^{\mu_5}\phi'_{5i}\phi'_{5j}q_{5j}\right) \\ & + EI_{23}\left(\sum_{j=1}^{\mu_3}\phi'_{5i}\phi'_{3j}q_{3j}\right) \\ & + k_3AG\left(\sum_{j=1}^{\mu_5}\phi_{5i}\phi_{5j}q_{5j} - \sum_{j=1}^{\mu_4}\phi_{5i}\phi'_{4j}q_{4j}\right)\Bigg]dx\end{aligned} \tag{19}$$

2.3 The kinetic energy of the system

The velocity vector $\mathbf{v}$ of an arbitrary point Q in the beam (see Fig. 2) is given by

$$\mathbf{v} = \frac{d\mathbf{r}}{dt} + \Omega\mathbf{k}\times\mathbf{r} \tag{20}$$

where Ω is the angular velocity of the rotating hub, and $\mathbf{r}$ is the vector from the center of the hub to point Q. Using the coordinate system fixed to the rigid hub, $\mathbf{r}$ can be expressed as follows:

$$\mathbf{r} = (r + x + u_1 - z\theta_3 - y\theta_2)\mathbf{i} + (y + u_2)\mathbf{j} + (z + u_3)\mathbf{k} \tag{21}$$

where r is the radius of the rigid hub.

Substituting Eq. (21) into Eq. (20), one obtains the velocity at point Q, as

$$\mathbf{v} = v_1\mathbf{i} + v_2\mathbf{j} + v_3\mathbf{k} \tag{22}$$

where

$$v_1 = \dot{u}_1 - z\dot{\theta}_3 - y\dot{\theta}_2 - \Omega(y + u_2) \tag{23}$$

$$v_2 = \dot{u}_2 + \Omega(r + x + u_1 - z\theta_3 - y\theta_2) \tag{24}$$

$$v_3 = \dot{u}_3 \tag{25}$$

Using Eq. (22), the kinetic energy of the rotating beam is derived as shown below.

$$\begin{aligned}T &= \frac{1}{2}\int_V \frac{\rho}{A}\mathbf{v}\cdot\mathbf{v}dV \\ &= \frac{1}{2}\int_0^L \frac{\rho}{A}\int_A (v_1^2 + v_2^2 + v_3^2)dAdx\end{aligned} \tag{26}$$

in which, V is the volume, A is the cross-section, and ρ is the mass density per unit length of the beam, respectively.

Using Eqs. (23)–(25) in Eq. (26), the kinetic energy becomes,

$$T = T_1 + T_2 + T_3 \tag{27}$$

where

$$\begin{aligned}T_1 = \frac{1}{2}\int_0^L \rho\Bigg(&\dot{u}_1^2 + \frac{I_2}{A}\dot{\theta}_3^2 + \frac{I_3}{A}\dot{\theta}_2^2 + \frac{I_3}{A}\Omega^2 + \Omega^2u_2^2 \\ &-2\Omega u_2\dot{u}_1 + \frac{2I_{23}}{A}\dot{\theta}_2\dot{\theta}_3 + \frac{2\Omega I_{23}}{A}\dot{\theta}_3 + \frac{2\Omega I_3}{A}\dot{\theta}_2\Bigg)dx\end{aligned} \tag{28}$$

$$\begin{aligned}T_2 = \frac{1}{2}\int_0^L \rho\Bigg[&\dot{u}_2^2 + \Omega^2(r + x + u_1)^2 + 2\Omega\dot{u}_2(r + x + u_1) \\ &+\Omega^2\left(\frac{I_2}{A}\theta_3^2 + \frac{I_3}{A}\theta_2^2 + \frac{2I_{23}}{A}\theta_2\theta_3\right)\Bigg]dx\end{aligned} \tag{29}$$

$$T_3 = \frac{1}{2}\int_0^L \rho\dot{u}_3^2dx \tag{30}$$

To derive the equations of motion, the partial derivatives of T with respect to the generalized coordinates q_{ij} and generalized velocities $\dot{q}_{ij}$ are needed. The derivatives of $\frac{\partial T}{\partial\dot{q}_{ij}}$'s with respect to t are also needed. Substituting Eqs. (2)–(7)

into Eqs. (27)–(30), taking derivatives with respect to q_{ij} and $\dot{q}_{ij}$, and neglecting higher order non-linear terms, one has

$$\frac{\partial T}{\partial q_{1i}} = \int_0^L \rho\Omega \left[\Omega(r+x)\phi_{1i} + \Omega \sum_{j=1}^{\mu_1} \phi_{1i}\phi_{1j} q_{1j} + \sum_{j=1}^{\mu_2} \phi_{1i}\phi_{2j}\dot{q}_{2j} \right] dx \tag{31}$$

$$\frac{\partial T}{\partial q_{2i}} = \int_0^L \rho\Omega \left(\Omega \sum_{j=1}^{\mu_2} \phi_{2i}\phi_{2j} q_{2j} - \sum_{j=1}^{\mu_1} \phi_{2i}\phi_{1j}\dot{q}_{1j} \right) dx - \int_0^L \rho\Omega^2 \left[r(L-x) + \frac{1}{2}\left(L^2 - x^2\right) \right] \cdot \sum_{j=1}^{\mu_2} \phi'_{2i}\phi'_{2j} q_{2j} dx \tag{32}$$

$$\frac{\partial T}{\partial q_{3i}} = \int_0^L \rho\Omega^2 \left(\frac{I_3}{A} \sum_{j=1}^{\mu_3} \phi_{3i}\phi_{3j} q_{3j} + \frac{I_{23}}{A} \sum_{j=1}^{\mu_5} \phi_{3i}\phi_{5j} q_{5j} \right) dx \tag{33}$$

$$\frac{\partial T}{\partial q_{4i}} = -\int_0^L \rho\Omega^2 \left[r(L-x) + \frac{1}{2}\left(L^2 - x^2\right) \right] \cdot \sum_{j=1}^{\mu_4} \phi'_{4i}\phi'_{4j} q_{4j} dx \tag{34}$$

$$\frac{\partial T}{\partial q_{5i}} = \int_0^L \rho\Omega^2 \left(\frac{I_2}{A} \sum_{j=1}^{\mu_5} \phi_{5i}\phi_{5j} q_{5j} + \frac{I_{23}}{A} \sum_{j=1}^{\mu_3} \phi_{5i}\phi_{3j} q_{3j} \right) dx \tag{35}$$

$$\frac{d}{dt}\frac{\partial T}{\partial \dot{q}_{1i}} = \int_0^L \rho \left(\sum_{j=1}^{\mu_1} \phi_{1i}\phi_{1j}\ddot{q}_{1j} - \Omega \sum_{j=1}^{\mu_2} \phi_{1i}\phi_{2j}\dot{q}_{2j} \right) dx \tag{36}$$

$$\frac{d}{dt}\frac{\partial T}{\partial \dot{q}_{2i}} = \int_0^L \rho \left(\sum_{j=1}^{\mu_2} \phi_{2i}\phi_{2j}\ddot{q}_{2j} + \Omega \sum_{j=1}^{\mu_1} \phi_{2i}\phi_{1j}\dot{q}_{1j} \right) dx \tag{37}$$

$$\frac{d}{dt}\frac{\partial T}{\partial \dot{q}_{3i}} = \int_0^L \rho \left(\frac{I_3}{A} \sum_{j=1}^{\mu_3} \phi_{3i}\phi_{3j}\ddot{q}_{3j} + \frac{I_{23}}{A} \sum_{j=1}^{\mu_5} \phi_{3i}\phi_{5j}\ddot{q}_{5j} \right) dx \tag{38}$$

$$\frac{d}{dt}\frac{\partial T}{\partial \dot{q}_{4i}} = \int_0^L \rho \sum_{j=1}^{\mu_4} \phi_{4i}\phi_{4j}\ddot{q}_{4j} dx \tag{39}$$

$$\frac{d}{dt}\frac{\partial T}{\partial \dot{q}_{5i}} = \int_0^L \rho \left(\frac{I_2}{A} \sum_{j=1}^{\mu_5} \phi_{5i}\phi_{5j}\ddot{q}_{5j} + \frac{I_{23}}{A} \sum_{j=1}^{\mu_3} \phi_{5i}\phi_{3j}\ddot{q}_{3j} \right) dx \tag{40}$$

2.4 Equations of motion

The Lagrange's equations of motion for free vibration of a distributed parameter system are given by [36]

$$\frac{d}{dt}\left(\frac{\partial T}{\partial \dot{q}_i}\right) - \frac{\partial T}{\partial q_i} + \frac{\partial U}{\partial q_i} = 0 \quad i = 1, 2, \ldots, \mu \tag{41}$$

where μ is the total number of modal coordinates, and T and U the kinetic energy and potential energy of the beam, respectively.

By substituting Eqs. (31)–(40) into Eq. (41), the linearized equations of motion can be obtained as follows

$$\sum_{j=1}^{\mu_1} M_{ij}^{11}\ddot{q}_{1j} - 2\Omega \sum_{j=1}^{\mu_2} M_{ij}^{12}\dot{q}_{2j} + \sum_{j=1}^{\mu_1} \left(K_{ij}^{S} - \Omega^2 M_{ij}^{11} \right) q_{1j} = r\Omega^2 P_{1i} + \Omega^2 Q_{1i}, \quad i = 1, 2, \ldots, \mu_1 \tag{42}$$

$$\sum_{j=1}^{\mu_2} M_{ij}^{22}\ddot{q}_{2j} + 2\Omega \sum_{j=1}^{\mu_1} M_{ij}^{21}\dot{q}_{1j} + \sum_{j=1}^{\mu_2} \left[K_{ij}^{B2} + \Omega^2 \left(M_{ij}^{\rho 2} - M_{ij}^{22} \right) \right] q_{2j} - \sum_{j=1}^{\mu_3} K_{ij}^{C23} q_{3j} = 0, \quad i = 1, 2, \ldots, \mu_2 \tag{43}$$

$$\sum_{j=1}^{\mu_3} M_{ij}^{I3}\ddot{q}_{3j} + \sum_{j=1}^{\mu_5} M_{ij}^{I35}\ddot{q}_{5j} - \sum_{j=1}^{\mu_2} K_{ij}^{D32} q_{2j} + \sum_{j=1}^{\mu_3} \left(K_{ij}^{I3} + K_{ij}^{A3} - \Omega^2 M_{ij}^{I3} \right) q_{3j} + \sum_{j=1}^{\mu_5} \left(K_{ij}^{I35} - \Omega^2 M_{ij}^{I35} \right) q_{5j} = 0, \quad i = 1, 2, \ldots, \mu_3 \tag{44}$$

$$\sum_{j=1}^{\mu_4} M_{ij}^{44}\ddot{q}_{4j} + \sum_{j=1}^{\mu_4} \left(K_{ij}^{B4} + \Omega^2 M_{ij}^{\rho 4} \right) q_{4j} - \sum_{j=1}^{\mu_5} K_{ij}^{C45} q_{5j} = 0, \quad i = 1, 2, \ldots, \mu_4 \tag{45}$$

$$\sum_{j=1}^{\mu_3} M_{ij}^{I53}\ddot{q}_{3j} + \sum_{j=1}^{\mu_5} M_{ij}^{I5}\ddot{q}_{5j} + \sum_{j=1}^{\mu_3}\left(K_{ij}^{I53} - \Omega^2 M_{ij}^{I53}\right) q_{3j} - \sum_{j=1}^{\mu_4} K_{ij}^{D54} q_{4j} + \sum_{j=1}^{\mu_5}\left(K_{ij}^{I5} + K_{ij}^{A5} - \Omega^2 M_{ij}^{I5}\right) q_{5j} = 0, \quad i = 1, 2, \ldots, \mu_5 \tag{46}$$

where

$$M_{ij}^{mn} = \int_0^L \rho\phi_{mi}\phi_{nj}dx \tag{47}$$

$$M_{ij}^{I3} = \int_0^L \frac{\rho I_3}{A}\phi_{3i}\phi_{3j}dx \tag{48}$$

$$M_{ij}^{I5} = \int_0^L \frac{\rho I_2}{A}\phi_{5i}\phi_{5j}dx \tag{49}$$

$$M_{ij}^{Imn} = \int_0^L \frac{\rho I_{23}}{A}\phi_{mi}\phi_{nj}dx \tag{50}$$

$$M_{ij}^{\rho n} = \int_0^L \rho\left[r(L-x) + \frac{1}{2}\left(L^2 - x^2\right)\right]\phi'_{ni}\phi'_{nj}dx \tag{51}$$

$$K_{ij}^{I3} = \int_0^L EI_3\phi'_{3i}\phi'_{3j}dx \tag{52}$$

$$K_{ij}^{I5} = \int_0^L EI_2\phi'_{5i}\phi'_{5j}dx \tag{53}$$

$$K_{ij}^{Imn} = \int_0^L EI_{23}\phi'_{mi}\phi'_{nj}dx \tag{54}$$

$$K_{ij}^{A3} = \int_0^L k_2 AG\phi_{3i}\phi_{3j}dx \tag{55}$$

$$K_{ij}^{B2} = \int_0^L k_2 AG\phi'_{2i}\phi'_{2j}dx \tag{56}$$

$$K_{ij}^{C23} = \int_0^L k_2 AG\phi'_{2i}\phi_{3j}dx \tag{57}$$

$$K_{ij}^{D32} = \int_0^L k_2 AG\phi_{3i}\phi'_{2j}dx \tag{58}$$

$$K_{ij}^{A5} = \int_0^L k_3 AG\phi_{5i}\phi_{5j}dx \tag{59}$$

$$K_{ij}^{B4} = \int_0^L k_3 AG\phi'_{4i}\phi'_{4j}dx \tag{60}$$

$$K_{ij}^{C45} = \int_0^L k_3 AG\phi'_{4i}\phi_{5j}dx \tag{61}$$

$$K_{ij}^{D54} = \int_0^L k_3 AG\phi_{5i}\phi'_{4j}dx \tag{62}$$

$$K_{ij}^{S} = \int_0^L EA\phi'_{1i}\phi'_{1j}dx \tag{63}$$

$$P_{1i} = \int_0^L \rho\phi_{1i}dx \tag{64}$$

$$Q_{1i} = \int_0^L \rho x\phi_{1i} \tag{65}$$

The coupling effect between the bending and stretching motions is ignored in the present study, as these gyroscopic coupling terms are often assumed to have negligible effects on the end results [32]. When the coupling effect between stretching and bending is ignored, the equations of motion can be simplified as

$$\sum_{j=1}^{\mu_2} M_{ij}^{22}\ddot{q}_{2j} + \sum_{j=1}^{\mu_2}\left[K_{ij}^{B2} + \Omega^2\left(M_{ij}^{\rho 2} - M_{ij}^{22}\right)\right] q_{2j} - \sum_{j=1}^{\mu_3} K_{ij}^{C23} q_{3j} = 0, \quad i = 1, 2, \ldots, \mu_2 \tag{66}$$

$$\sum_{j=1}^{\mu_3} M_{ij}^{I3}\ddot{q}_{3j} + \sum_{j=1}^{\mu_5} M_{ij}^{I35}\ddot{q}_{5j} - \sum_{j=1}^{\mu_2} K_{ij}^{D32} q_{2j} + \sum_{j=1}^{\mu_3}\left(K_{ij}^{I3} + K_{ij}^{A3} - \Omega^2 M_{ij}^{I3}\right) q_{3j} + \sum_{j=1}^{\mu_5}\left(K_{ij}^{I35} - \Omega^2 M_{ij}^{I35}\right) q_{5j} = 0, \quad i = 1, 2, \ldots, \mu_3 \tag{67}$$

$$\sum_{j=1}^{\mu_4} M_{ij}^{44}\ddot{q}_{4j} + \sum_{j=1}^{\mu_4}\left(K_{ij}^{B4} + \Omega^2 M_{ij}^{\rho 4}\right) q_{4j} - \sum_{j=1}^{\mu_5} K_{ij}^{C45} q_{5j} = 0, \quad i = 1, 2, \ldots, \mu_4 \tag{68}$$

$$\sum_{j=1}^{\mu_3} M_{ij}^{I53}\ddot{q}_{3j} + \sum_{j=1}^{\mu_5} M_{ij}^{I5}\ddot{q}_{5j} + \sum_{j=1}^{\mu_3}\left(K_{ij}^{I53} - \Omega^2 M_{ij}^{I53}\right) q_{3j} - \sum_{j=1}^{\mu_4} K_{ij}^{D54} q_{4j} + \sum_{j=1}^{\mu_5}\left(K_{ij}^{I5} + K_{ij}^{A5} - \Omega^2 M_{ij}^{I5}\right) q_{5j} = 0, \quad i = 1, 2, \ldots, \mu_5 \tag{69}$$

3 Dimensionless transformation

If the cross-sectional properties of the beam remain constant, it is useful to rewrite the equations of motion in a dimensionless form. For this transformation several dimensionless variables and parameters are defined as follows [32]:

$$\tau = \frac{t}{T} \tag{70}$$

$$\xi = \frac{x}{L} \tag{71}$$

$$\theta_{ij} = \frac{q_{ij}}{L} \tag{72}$$

$$\gamma = \Omega T \tag{73}$$

$$\delta = \frac{r}{L} \tag{74}$$

$$\kappa = \frac{I_2^*}{I_3^*} \tag{75}$$

where T is defined as

$$T = \sqrt{\frac{\rho L^4}{E I_3^*}} \tag{76}$$

The variables γ, δ and κ represent the angular speed ratio, the hub radius ratio and the principal area moment of inertia ratio, respectively. By using the parameter κ defined above, Eqs. (10)–(12) for calculating the second area moments can be written as [32]

$$\frac{I_3}{I_3^*} = \frac{1}{2}(\kappa + 1) - \frac{1}{2}(\kappa - 1)\cos(2\alpha\xi) \tag{77}$$

$$\frac{I_2}{I_3^*} = \frac{1}{2}(\kappa + 1) + \frac{1}{2}(\kappa - 1)\cos(2\alpha\xi) \tag{78}$$

$$\frac{I_{23}}{I_3^*} = \frac{1}{2}(\kappa - 1)\sin(2\alpha\xi). \tag{79}$$

Substituting the dimensionless variables and parameters defined in Eqs. (70)–(75) into Eqs. (43)–(46), the dimensionless equations of motion can be written as

$$\sum_{j=1}^{\mu_2} \overline{M}_{ij}^{22}\ddot{\theta}_{2j} + \sum_{j=1}^{\mu_2}\left[\eta_2\beta^2\overline{K}_{ij}^{B2} + \gamma^2\left(\overline{M}_{ij}^{\rho 2} - \overline{M}_{ij}^{22}\right)\right]\theta_{2j} - \eta_2\beta^2\sum_{j=1}^{\mu_3}\overline{K}_{ij}^{C23}\theta_{3j} = 0, \quad i = 1, 2, \ldots, \mu_2 \tag{80}$$

$$\sum_{j=1}^{\mu_3} \overline{M}_{ij}^{I3}\ddot{\theta}_{3j} + \sum_{j=1}^{\mu_5} \overline{M}_{ij}^{I35}\ddot{\theta}_{5j} - \eta_2\beta^4\sum_{j=1}^{\mu_2}\overline{K}_{ij}^{D32}\theta_{2j} + \sum_{j=1}^{\mu_3}\left(\beta^2\overline{K}_{ij}^{I3} + \eta_2\beta^4\overline{K}_{ij}^{A3} - \gamma^2\overline{M}_{ij}^{I3}\right)\theta_{3j} + \sum_{j=1}^{\mu_5}\left(\beta^2\overline{K}_{ij}^{I35} - \gamma^2\overline{M}_{ij}^{I35}\right)\theta_{5j} = 0, \quad i = 1, 2, \ldots, \mu_3 \tag{81}$$

$$\sum_{j=1}^{\mu_4} \overline{M}_{ij}^{44}\ddot{\theta}_{4j} + \sum_{j=1}^{\mu_4}\left(\eta_3\beta^2\overline{K}_{ij}^{B4} + \gamma^2\overline{M}_{ij}^{\rho 4}\right)\theta_{4j} - \eta_3\beta^2\sum_{j=1}^{\mu_5}\overline{K}_{ij}^{C45}\theta_{5j} = 0, \quad i = 1, 2, \ldots, \mu_4 \tag{82}$$

$$\sum_{j=1}^{\mu_3} \overline{M}_{ij}^{I53}\ddot{\theta}_{3j} + \sum_{j=1}^{\mu_5} \overline{M}_{ij}^{I5}\ddot{\theta}_{5j} + \sum_{j=1}^{\mu_3}\left(\beta^2\overline{K}_{ij}^{I53} - \gamma^2\overline{M}_{ij}^{I53}\right)\theta_{3j} - \eta_3\beta^4\sum_{j=1}^{\mu_4}\overline{K}_{ij}^{D54}\theta_{4j} + \sum_{j=1}^{\mu_5}\left(\beta^2\overline{K}_{ij}^{I5} + \eta_3\beta^4\overline{K}_{ij}^{A5} - \gamma^2\overline{M}_{ij}^{I5}\right)\theta_{5j} = 0, \quad i = 1, 2, \ldots, \mu_5 \tag{83}$$

where

$$\beta = \sqrt{\frac{AL^2}{I_3^*}} \tag{84}$$

$$\eta_2 = \frac{k_2 G}{E} \tag{85}$$

$$\eta_3 = \frac{k_3 G}{E} \tag{86}$$

$$\overline{M}_{ij}^{mn} = \int_0^1 \psi_{mi}\psi_{nj}\,d\xi \tag{87}$$

$$\overline{M}_{ij}^{I3} = \int_0^1 \left[\frac{1}{2}(\kappa + 1) - \frac{1}{2}(\kappa - 1)\cos(2\alpha\xi)\right]\psi_{3i}\psi_{3j}\,d\xi \tag{88}$$

Table 1 Convergence of the first three flapwise natural frequencies, using the modes of a cantilever beam as test functions. ($\alpha = 0, \beta = 50, \gamma = 8, \delta = 0, \kappa = 1, \eta = 0.25$)

Number of modes	1st Mode		2nd Mode		3rd Mode	
	Freq.	Error (%)[a]	Freq.	Error (%)	Freq.	Error (%)
1	9.2696	0.647				
2	9.2361	0.287	29.4949	0.588		
3	9.2263	0.181	29.4468	0.426	66.7950	0.779
4	9.2220	0.134	29.4039	0.280	66.7405	0.698
5	9.2195	0.107	29.4003	0.268	66.6116	0.506
6	9.2197	0.110	29.3835	0.211	66.5968	0.484
7	9.2168	0.078	29.3787	0.195	66.5272	0.379
8	9.2160	0.069	29.3696	0.164	66.5175	0.365
9	9.2153	0.062	29.3665	0.153	66.4764	0.303
10	9.2132	0.039	29.3501	0.097	66.4010	0.190

[a] Based on the first three natural frequencies, 9.2096, 29.3215 and 66.2748 from [14]

$$\overline{M}_{ij}^{I5} = \int_0^1 \left[\frac{1}{2}(\kappa+1) + \frac{1}{2}(\kappa-1)\cos(2\alpha\xi)\right]\psi_{5i}\psi_{5j}d\xi \tag{89}$$

$$\overline{M}_{ij}^{Imn} = \int_0^1 \frac{1}{2}(\kappa-1)\sin(2\alpha\xi)\psi_{mi}\psi_{nj}d\xi \tag{90}$$

$$\overline{M}_{ij}^{\rho n} = \int_0^1 \left[\delta(1-\xi) + \frac{1}{2}(1-\xi^2)\right]\psi'_{ni}\psi'_{nj}d\xi \tag{91}$$

$$\overline{K}_{ij}^{I3} = \int_0^1 \left[\frac{1}{2}(\kappa+1) - \frac{1}{2}(\kappa-1)\cos(2\alpha\xi)\right]\psi'_{3i}\psi'_{3j}d\xi \tag{92}$$

$$\overline{K}_{ij}^{I5} = \int_0^1 \left[\frac{1}{2}(\kappa+1) + \frac{1}{2}(\kappa-1)\cos(2\alpha\xi)\right]\psi'_{5i}\psi'_{5j}d\xi \tag{93}$$

$$\overline{K}_{ij}^{Imn} = \int_0^1 \frac{1}{2}(\kappa-1)\sin(2\alpha\xi)\psi'_{mi}\psi'_{nj}d\xi \tag{94}$$

$$\overline{K}_{ij}^{An} = \int_0^1 \psi_{ni}\psi_{nj}d\xi \tag{95}$$

$$\overline{K}_{ij}^{Bn} = \int_0^1 \psi'_{ni}\psi'_{nj}d\xi \tag{96}$$

$$\overline{K}_{ij}^{Cmn} = \int_0^1 \psi'_{mi}\psi_{nj}d\xi \tag{97}$$

$$\overline{K}_{ij}^{Dmn} = \int_0^1 \psi_{mi}\psi'_{nj}d\xi \tag{98}$$

where ψ_{ij} are the normalized assumed modal functions of ξ, and $(\,)'$ denotes the derivative with respect to ξ.

The parameter β is the slenderness ratio of the Timoshenko beam, and η_2 and η_3 are the effective shear to tensile stiffness ratios (including the effect of the shear correction factors). It should be noted that the shear correction factors k_2 and k_3 are different for shear in the $x-y$ and $x-z$ planes, and they may not be constant along the length of the beam. In the present study, in order to obtain the dimensionless equations of motion, we approximately assumed that these two factors are constant along the x-direction. It should be noted that there are numerous definitions and recommended values for the shear correction factor in published papers. Different definitions will yield different values for the shear correction factor. The shear correction factor is a function of the cross-section and, depending on the interpretation, may also be a function of the Poisson ratio. Different approaches for estimating the shear correction factor can be found, for examples, in [35,37–39].

4 Numerical results

In order to obtain accurate numerical results, several assumed modes are used to construct the matrices defined in Eqs. (80)–(83). Any compact set of functions which satisfy the essential boundary conditions of the Timoshenko beam can be used as the test functions. The normalized modes of a non-rotating Euler–Bernoulli cantilever beam, the orthogonal Legendre polynomials, the polynomial comparison functions, etc. can

Table 2 Convergence of the first three flapwise natural frequencies, using the Legendre polynomials as test functions ($\alpha = 0, \beta = 50, \gamma = 8, \delta = 0, \kappa = 1, \eta = 0.25$)

Number of modes	1st Mode		2nd Mode		3rd Mode	
	Freq.	Error (%)[a]	Freq.	Error (%)	Freq.	Error (%)
1	9.2786	0.744				
2	9.2455	0.388	29.5240	0.686		
3	9.2356	0.282	29.4760	0.524	66.8614	0.877
4	9.2309	0.231	29.4331	0.379	66.8070	0.797
5	9.2285	0.205	29.4265	0.357	66.6779	0.605
6	9.2276	0.195	29.4126	0.310	66.6631	0.582
7	9.2261	0.179	29.4080	0.294	66.5933	0.478
8	9.2253	0.170	29.3989	0.263	66.5805	0.459
9	9.2236	0.152	29.3944	0.248	66.5401	0.399
10	9.2217	0.131	29.3785	0.194	66.4635	0.284

[a] Based on the first three natural frequencies, 9.2096, 29.3215 and 66.2748 from [14]

Table 3 Comparison of the first four natural frequencies for a non-rotating beam ($\gamma = 0, \kappa = 0.25, \eta = 0.25, \beta = 1{,}000$)

α (°)	Present	Ref. [17]	Ref. [18]	Ref. [32]
First				
30	1.7622	1.7630	1.7620	1.7623
60	1.7748	1.7737	1.7742	1.7748
90	1.7950	1.7948	1.7949	1.7950
Second				
30	3.4793	3.4788	3.4787	3.4793
60	3.3798	3.3790	3.3790	3.3799
90	3.2426	3.2422	3.2426	3.2425
Third				
30	11.1690	11.1681	11.1698	11.1693
60	11.6040	11.6025	11.6064	11.6046
90	12.2644	12.2631	12.2611	12.2649
Fourth				
30	21.4470	21.4451	21.4568	21.4489
60	20.1531	20.1497	20.1769	20.1545
90	18.7301	18.7246	18.7661	18.7307

be used as test functions in the numerical calculation. Also, to focus on the critical effects on the modal characteristics due to rotation and slenderness ratio, we assume that the shear correction factors k_2 and k_3 are the same in the following computation. The case $k_2 = k_3$ is relevant only for circular and quadratic cross-sections This assumption is valid for a beam made of isotropic materials with a circular or quadratic cross-section. For other cross-sections, both k_2 and k_3 need to be estimated (see [35,37–39]).

The convergence of the first three flapwise frequencies of a rotating Timoshenko beam is shown in Table 1 using the normalized modes of a non-rotating Euler–Bernoulli cantilever beam as test functions, and in Table 2 using the orthogonal Legendre polynomials as test functions. The "number of modes" in the tables represents the number of assumed modes for each individual deformation variable. It can be seen that using ten modes for each individual deformation variable is sufficient to obtain a reasonable accuracy for the first three natural frequencies. Moreover, the results show good agreement between the natural frequencies obtained in this study using the normalized modes of a non-rotating Euler–Bernoulli cantilever beam and the orthogonal Legendre polynomials as test functions.

In the following examples, the normalized modes of a non-rotating Euler–Bernoulli cantilever beam will be used as test functions.

To verify the accuracy of the present modeling method. The numerical results from the present modeling method

Table 4 Comparison of the first four flapwise natural frequencies for a rotating beam ($\alpha = 0, \delta = 0, \kappa = 1, \eta = 0.25$)

γ	0		4		8		10	
β	Present	Ref. [14]	Present	Ref. [14]	Present	Ref. [14]	Present	Ref. [14]
Euler	3.5059	3.5160	5.5850	5.5850	9.2568	9.2568	13.1704	13.1702
	22.0296	22.0345	24.2726	24.2733	29.9950	29.9954	37.6037	37.6031
	61.8502	61.6971	63.9627	63.9666	70.2896	70.2929	79.6136	79.6144
	120.2983	120.9010	123.2354	123.2610	130.0251	30.0490	40.5155	140.5340
50	3.5000	3.4998	5.5623	5.5616	9.2132	9.2096	13.0972	13.0870
	21.3692	21.3547	23.6240	23.6061	29.3501	29.3215	36.9140	36.8659
	57.5636	57.4705	59.9130	59.8117	66.4010	66.2748	75.8382	75.6698
	107.2812	106.9260	109.8286	09.4590	117.0778	116.6650	128.0863	127.6040
25	3.4534	3.4527	5.4980	5.4951	9.0975	9.0854	12.9229	12.8934
	19.6965	19.6497	22.0126	21.9557	27.7933	27.7082	35.3077	35.1811
	49.1256	48.8891	51.7372	51.4822	58.7562	58.4507	68.6107	68.2339
	84.8053	84.1133	87.9002	87.1836	96.4247	95.6423	108.7570	107.8870
16.67	3.3803	3.3787	5.4013	5.3954	8.9423	8.9209	12.7180	12.6724
	17.6251	17.5470	20.0593	19.9662	25.9651	25.8362	33.4388	33.2672
	41.0522	40.7447	44.0648	43.7365	51.7950	51.4154	62.0432	61.6011
	67.0789	66.3623	70.8683	70.1298	80.7277	79.9414	93.8868	93.0672
12.5	3.2863	3.2837	5.2840	5.2749	8.7746	8.7456	12.5134	12.4581
	15.5873	15.4883	18.1781	18.0628	24.1961	24.0479	31.4634	31.2846
	34.6138	34.3005	38.0639	37.7317	46.3420	45.9683	56.3909	55.9744
	54.2503	53.6516	58.5494	57.9491	68.3629	67.8215	77.4992	77.1047
10	3.1774	3.1738	5.1570	5.1448	8.6077	8.5735	12.3066	12.2467
	13.7694	13.6607	16.5184	16.3946	22.4979	22.3506	29.0691	28.9100
	29.6487	29.3614	33.4810	33.1793	41.7829	41.4632	49.9746	49.6484
	44.3234	43.9102	48.1460	47.8101	53.5041	53.2833	56.9137	56.6750

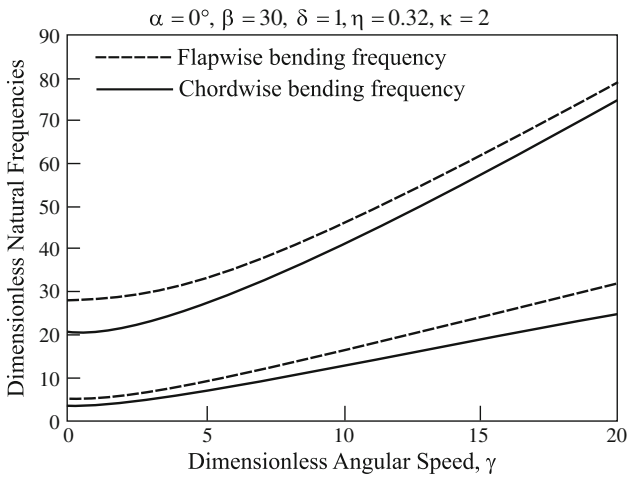

Fig. 3 No intersection of the first four natural frequencies of a non-twisted beam when $\kappa > 1$

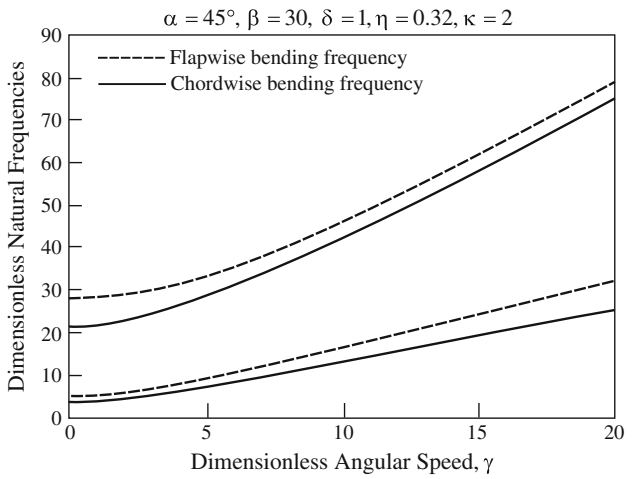

Fig. 4 No intersection of the first four natural frequencies of a twisted beam when $\kappa > 1$

are compared with those presented in Refs. [17,18,32] for a rotating pre-twisted Euler–Bernoulli beam. For this examples, a typical metallic material with a Poisson's ratio of 0.333 is used such that $E/G = 2.667$. Using a shear correction factor defined by Cowper [37] of 0.85 for a rectangular cross-section, the effective shear to axial stiffness ratio

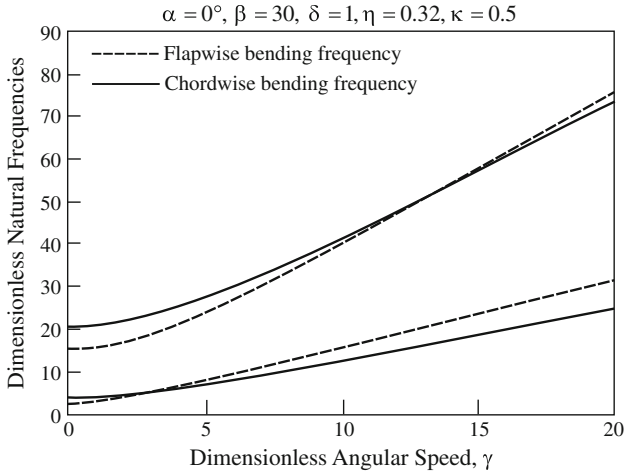

Fig. 5 Intersection of the first four natural frequencies of a non-twisted beam when $\kappa < 1$

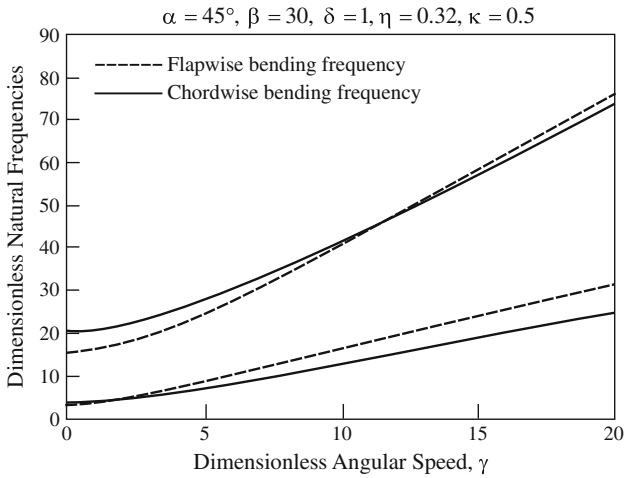

Fig. 6 Intersection of the first four natural frequencies of a twisted beam when $\kappa < 1$

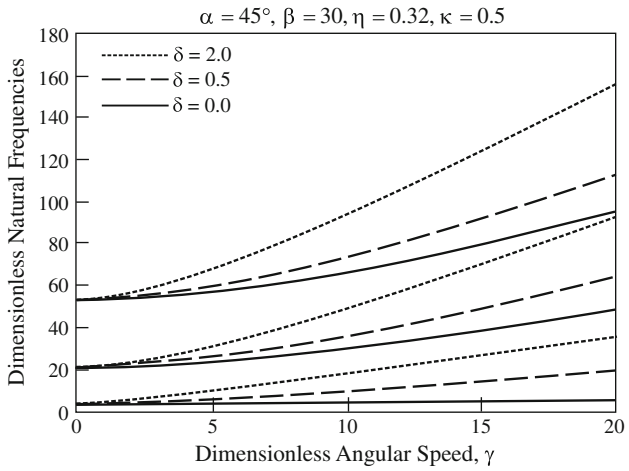

Fig. 7 The effect of the hub radius ratio on the first three natural frequencies

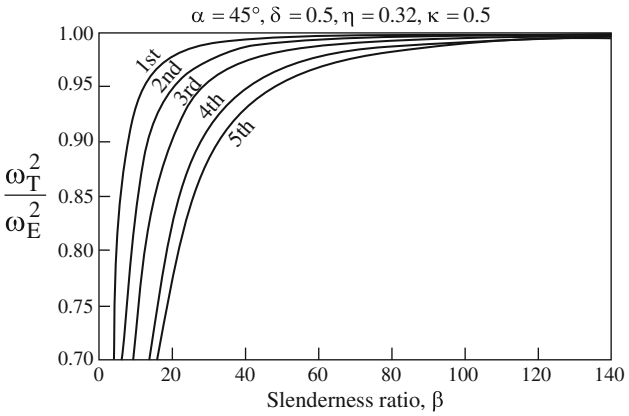

Fig. 8 The effect of the slenderness ratio on the first five natural frequencies

η then becomes 0.32. Please note that there are numerous definitions of k in published papers. In this example, the definition by Cowper was used in the calculation. Other popular values of k were given as 2/3 by Timoshenko [35], and 5/6 by Reissner [38]. The first four natural frequencies from the present method and those from [17,18,32] are listed in Table 3. The results obtained from the present method shows a maximum of 0.194% difference.

In Table 4, the flapwise natural frequencies from the present method and those from Ref. [14] are compared for a rotating Timoshenko beam with different slenderness ratios and different rotational speeds. The maximum relative error between the two sets of results is approximately 1.1%. In the calculation, assuming a shear correction factor of 2/3, the effective shear to axial stiffness ratio η becomes 0.25 for a metallic material with a Poisson's ratio of 0.333.

The loci of the first four natural frequencies of a rotating beam with no pre-twist are shown in Fig. 3. The loci of the flapwise and chordwise bending natural frequencies are drawn by dashed and solid lines, respectively. As expected, the natural frequencies increase as the rotational speed increases, due to the stiffening effect of the centrifugal force which is directly proportional to the square of the angular speed. Moreover, the loci of the flapwise and chordwise natural frequencies do not intersect, since the principal area moment of inertia (κ) is greater than 1. A similar result has also been observed for a pre-twisted beam with a 45° twist angle, as shown in Fig. 4.

In Figs. 5 and 6, the loci of the first four natural frequencies are presented for rotating beams with a pre-twist angle of 0° and 45°, respectively. All other parameters are kept the same as in Figs. 3 and 4 but the principal area moment of inertia ratio is smaller than one in the present case. Since κ is smaller than one, the flapwise bending frequencies are smaller than the chordwise bending frequencies when the

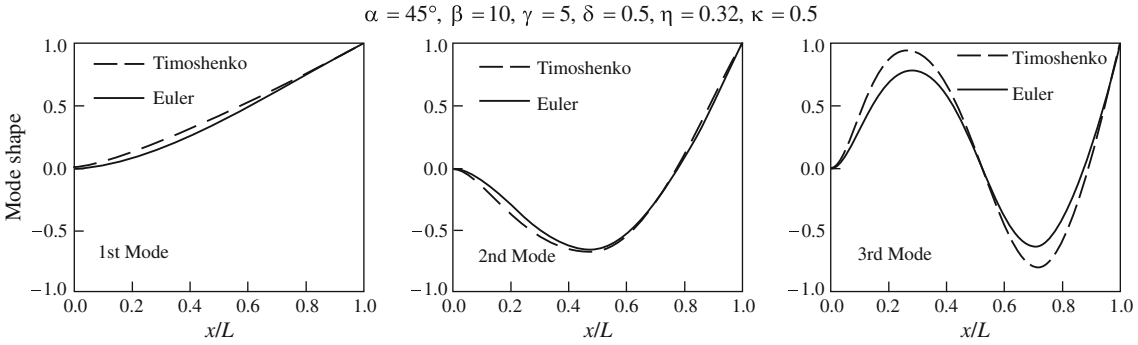

Fig. 9 Mode shape variation of the first three modes

Fig. 10 Tuned angular speeds

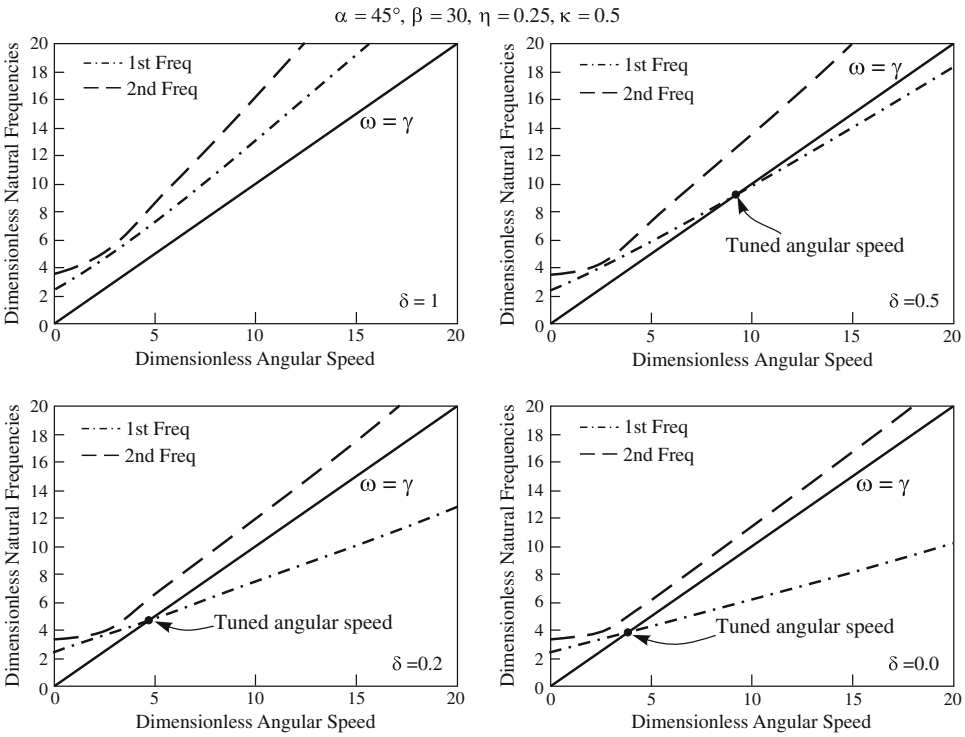

angular speed is zero. As the angular speed increases, the flapwise bending frequencies increase faster than the chordwise bending frequencies, thus causing the intersection between the loci of the flapwise bending frequencies and chordwise bending frequencies. However, the veering phenomena discussed in [32] for a rotating Euler–Bernoulli beam have not been observed in the present study for a rotating Timoshenko beam.

The loci of the first three natural frequencies are shown in Fig. 7 to investigate the effect of the hub radius ratio (δ). The slenderness ratio $\beta = 30$, the effective shear to axial stiffness ratio $\eta = 0.32$ and the principal area moment of inertia ratio $\kappa = 0.5$ are used in the simulation. Three hub radius ratios ($\delta = 0,\ 0.5,\ 2$) are considered in the calculation. As expected, the natural frequencies increase with the increasing rotational speed due to the stiffening effect of the centrifugal force that is directly proportional to Ω^2. Moreover, since the centrifugal force that is directly proportional to the hub radius makes the beam stiffer with the increasing hub radius ratio, the rate of increase of the natural frequencies increases as the hub radius ratio increases.

The effect of the slenderness ratio (β) on the natural frequencies is shown in Fig. 8 for a rotating beam with a pretwist angle of 45°. The ratios of the natural frequencies of a Timoshenko beam over the natural frequencies of an Euler–Bernoulli beam are depicted in the figure for the first five frequencies. It is seen that the natural frequencies increase as the slenderness ratio increases, and the natural frequencies of a Timoshenko beam are always lower than the natural frequencies of an Euler–Bernoulli beam. Moreover, it is noticed that the effect of the slenderness ratio is more significant on the higher modes than on the lower modes.

Table 5 The tuned angular speed versus κ, δ and $\alpha(\beta = 30, \eta = 0.25)$

δ	$\alpha = 0°$	$\alpha = 15°$	$\alpha = 30°$	$\alpha = 45°$
$\kappa = 0.5$				
0.0	3.7911	3.7870	3.7747	3.7548
0.1	4.1816	4.1778	4.1668	4.1485
0.2	4.7133	4.7100	4.7001	4.6836
0.3	5.4892	5.4863	5.4784	5.4646
0.4	6.7493	6.7472	6.7421	6.7326
0.5	9.2171	9.2170	9.2169	9.2168
$\kappa = 2.0$				
0.0	3.7911	3.7938	3.8019	3.8151
0.1	4.1816	4.1844	4.1929	4.2068
0.2	4.7133	4.7160	4.7246	4.7388
0.3	5.4892	5.4919	5.4997	5.5131
0.4	6.7493	6.7510	6.7562	6.7660
0.5	9.2171	9.2160	9.2129	9.2103

The differences of the first three mode shapes obtained from the Euler–Bernoulli and Timoshenko beam theories are shown in Fig. 9 when $\beta = 10$. Even though the natural frequencies from these two theories are significantly different, the mode shapes obtained from these two theories are noticeable, but not as significant even for a very short beam ($\beta = 10$).

Resonance will occur when the angular speed of the rotating beam equals one of the natural frequencies of the beam. The angular speed which causes the resonance is usually called the tuned angular speed [13].

Figure 10 shows the loci of the first two natural frequencies (for $\delta = 0$, $\delta = 0.2$, $\delta = 0.5$ and $\delta = 1$) and the straight line of $\omega = \gamma$. The tuned angular speed occurs when the loci of the natural frequencies intersect with the straight line of $\omega = \gamma$. It can be seen that the tuned angular speed occurs for $\delta = 0, 0.2, 0.5$, but it does not exist for $\delta = 1$.

The valuations of the tuned angular speed for rotating Timoshenko beams with various pre-twist angles, principal area moment of inertia ratios and hub radius ratios are listed in Table 5. It can be seen that the hub radius ratio is the most critical factor among these three dimensionless parameters.

For a rotating Timoshenko beam, the slenderness ratio will also affect the tuned angular speed. The variation of the tuned speed of rotating Timoshenko beams with various slenderness ratios are shown in Fig. 11. It is seen that the tuned angular speed increases when the slenderness ratio increases. Moreover, the rate of change of the tuned angular speed with respect to the slenderness ratio decreases with an increasing slenderness ratio; and there exists a asymptotic maximum tuned angular speed. The maximum tuned angular speeds when $\alpha = 45°$, $\delta = 0$ and $\eta = 0.25$ are approximately 3.837 for $\kappa = 0.5$ and 3.906 for $\kappa = 2$.

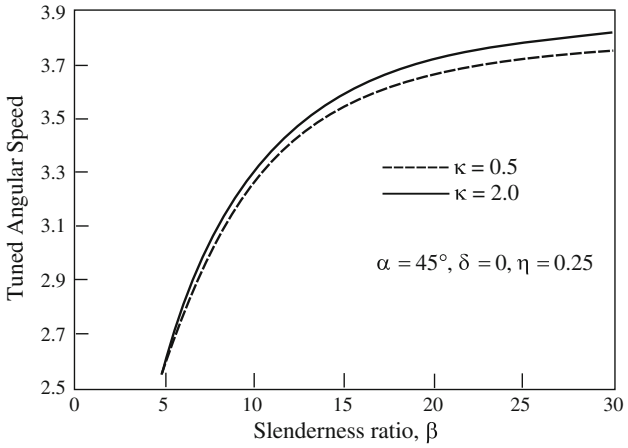

Fig. 11 The effect of the slenderness ratio on the tuned angular speed

5 Conclusions

In the present study, the equations of motion for the vibration analysis of rotating pre-twisted Timoshenko beams are derived using the hybrid deformation variables. The equations of motion are transformed into dimensionless forms in which the dimensionless parameters are identified.

The effects of the slenderness ratio, hub radius ratio, and rotational speed on the natural frequencies are investigated with the following results:

- The natural frequencies increase with the increasing rotational speed due to the stiffening effect of the centrifugal force induced from the rotation. Moreover, this effect is more significant on higher modes than on lower modes.
- The rate of increase of the natural frequencies increases as the hub radius ratio increases.
- The natural frequencies increase with an increasing slenderness ratio of a beam, and the natural frequencies of a Timoshenko beam are lower than those of an Euler–Bernoulli beam.
- The tuned angular speed exists, at which resonance may occur. For a rotating pre-twisted Timoshenko beam, all dimensionless parameters will affect the tuned angular speed, however, the hub radius ratio and the slenderness ratio are the two dominant factors in affecting the tuned angular speed.

References

1. Southwell R, Gough F (1921) The free transverse vibration of airscrew blades. Br ARC Rep Memoranda o.766
2. Liebers F (1930) Contribution to the theory of propeller vibration. NACA TM No. 568
3. Theodorsen T (1950) Propeller vibrations and the effect of centrigual force. NACA TN No. 516

4. Schilhansl M (1958) Bending frequency of rotating cantilever beam. J Appl Mech Trans Am Soc Mech Eng 25:28–30
5. Putter S, Manor H (1978) Natural frequencies of radial rotating beams. J Sound Vib 56:175–185
6. Hodges DH, Dowell EH (1974) Nonlinear equations of motion for the elastic bending and torsion of twisted nonuniform rotor blades. NASA TN D-7818
7. Hodges D (1979) Vibration and response of nonuniform rotating beams with discontinuities. J Am Helicopter Soc 24:43–50
8. Hoa J (1979) Vibration of a rotating beam with tip mass. J Sound Vib 67:369–381
9. Bhat R (1986) Transverse vibrations of a rotating uniform cantilever beam with tip mass as predicted by using beam characteristic orthogonal polynomials in the Rayleigh–Ritz method. J Sound Vib 105:199–210
10. Fox C, Burdress J (1979) The natural frequencies of a thin rotating cantilever with offset root. J Sound Vib 65:151–158
11. Yokoyama T (1988) Free vibration characteristics of rotating Timoshenko beams. Int J Mech Sci 30:743–755
12. Lee S, Lin S (1994) Bending vibrations of rotating nonuniform Timoshenko beams with an elastically restrained root. J Appl Mech 61:949–955
13. Yoo HH, Shin SH (1998) Vibration analysis of rotating cantilever beams. J Sound Vib 212:807–828
14. Ozgumus OO, Kaya MO (2008) Flapwise bending vibration analysis of a rotating double-tapered Timoshenko beam. Arch Appl Mech 78:379–392
15. Dawson B (1968) Coupled bending vibrations of pretwisted cantilever blading treated by Rayleigh–Ritz method. J Mech Eng Sci 10(5):381–386
16. Dawson B, Carnegie W (1969) Modal curves of pretwisted beams of rectangular cross-section. J Mech Eng Sci 11(1):1–13
17. Carnegie W, Thomas J (1972) The coupled bending-bending vibration of pre-twisted tapered blading. J Eng Indus 94:255–266
18. Dokumaci E, Thomas J, Carnegie W (1967) Matrix displacement analysis of coupled bending-bending vibrations of pre-twsited blading. J Mech Eng Sci 9:247–251
19. Rao JS (1992) Advanced theory of vibration. Wiley, New York
20. Gupta RS, Rao JS (1978) Finite element eigenvalue analysis of tapared and twisted timoshenko beams. J Sound Vib 56(2):187–200
21. Celep Z, Turhan D (1986) On the influence of pretwisting on the vibration of beams including the shear and rotatory inertia effects. J Sound Vib 110(3):523–528
22. Lin SM (1997) Vibrations of elastically restrained nonuniform beams with arbitrary pretwist. AIAA J 35(11):1681–1687
23. Ramamurti V, Kielb R (1984) Natural frequencies of twisted rotating plate. J Sound Vib 97:429–449
24. Subrahmanyam KB, Kaza KRV (1986) Vibration and buckling of rotating, pretwisted, preconed beams including coriolis effects. J Vib Acoustics Stress Reliab Des 108(2):140–149
25. Subrahmanyam KB, Kulkarni SV, Rao JS (1982) Analysis of lateral vibrations of rotating cantilever blades allowing for shear deflection and rotary inertia by reissner and potential energy methods. Mech Mach Theory 17(4):235–241
26. Lin SM (2001) The instability and vibration of rotating beams with arbitrary pretwist and an elastically restrained root. ASME J Appl Mech 68:844–853
27. Lin SM, Wu CT, Lee SY (2006) Analysis of rotating nonuniform pretwisted beams with an elastically restrained root and a tip mass. Int J Mech Sci 45:741–755
28. Frisch H (1975) A vector-dynamic development of the equations of motion for N-coupled flexible bodies and point masses. NASA TN D-8047
29. Ho J (1977) Direct path method for flexible multibody spacecraft dynamics. J Spacecrafts Rockets 14:102–110
30. Kane T, Ryan R, Banerjee A (1987) Dynamics of a cantilever beam attached to a moving base. J Guidance Control Dyn 10:139–151
31. Yoo H, Ryan R, Scott R (1995) Dynamics of flexible beam undergoing overall motions. J Sound Vib 181:261–278
32. Yoo HH, Park JH, Park J (2001) Vibration analysis of rotating pretwisted blades. Comput Struct 79:1811–1819
33. Yoo HH, Lee SH, Shin SH (2005) Flapwise bending vibration analysis of rotating multi-layered composite beams. J Sound Vib 286:745–761
34. Eisenhart L (1947) An Introduction to differential geometry. Princeton University Press, Princeton
35. Timoshenko S (1990) Vibration problems in engineering, 5th edn, Wiley. New York
36. Craig RR (1981) Structural dynamics: an introduction to computer methods. Wiley, New York
37. Cowper GR (1966) The shear coefficient in Timoshenko's beam theory. J Appl Mech 33(2):335–340
38. Reissner E (1945) The effect of transverse shear deformation on the bending of elastic plates. J Appl Mech 12:A68–A77
39. Vlachoutsis S (1992) Shear correction factors for plates and shells. Int J Numer Methods Eng 33(7):1537–1552